Universal scaling for ripple formation in granular media

F. Zoueshtiagh*
Laboratoire de Physique et Mécanique des Milieux Hétérogène (LPMMH), Ecole Supérieure de Physique et Chimie Industrielles (ESPCI), 10 Rue Vauquelin, 75231 Paris Cedex 05, France

P. J. Thomas†
Fluid Dynamics Research Centre, School of Engineering, University of Warwick, Coventry CV4 7AL, United Kingdom
(Received 17 July 2002; revised manuscript received 13 January 2003; published 25 March 2003)

The wavelength scaling of ripple patterns formed by granular materials underneath flowing fluids is investigated. Experimental results from five systems involving substantially different experimental conditions are compared to each other. The data analysis reveals that all systems display a common, global scaling behavior for the onset of ripple formation on short time scales. This suggests the existence of common physical mechanisms governing ripple formation in these systems.

DOI: 10.1103/PhysRevE.67.031301 PACS number(s): 45.70.Qj, 47.54.+r, 47.55.Kf, 92.10.Wa

I. INTRODUCTION

Ripple patterns are a characteristic feature associated with the flow of a gas or a liquid over an expanse of granular material. Typical examples are sand ripples in the desert or on the bottom of the ocean. Ripples can arise from different physical mechanisms. Various terminologies have been introduced to categorize patterns according to their appearance or their anticipated physical origins [1–5]. Specific terminologies exist, for instance, for ripples with different height to wavelength ratios or for ripples with different cross-sectional shape profiles emerging in steady, unidirectional or oscillatory flows. The details of the physical mechanisms leading to the formation of sand ripples are presently, at best, poorly understood.

In Ref. [6] we reported the observation of a spiral pattern established by a granular material underneath a rotating fluid. One typical example of this pattern is shown in Fig. 1—for further photographs refer to Refs. [6–10]. On the basis of comparisons between our experimental data and computations, together with some simple physical arguments, we speculated [9] that the spiral pattern might constitute a rotating analog of sand ripples. However, our previous publications on the subject did not contain any comparisons of our own experimental data for the spiral patterns with experimental data for granular ripple formation available in the literature. Hence, to date our conclusions of Ref. [9] have not been supported experimentally. Here we describe a detailed comparison between our own data [6–10] and results for fluvial sand ripples published in the literature [11–16].

Briefly, the spirals shown in Fig. 1 are formed by small granules (diameter 0.18–0.32 mm) on the bottom of a circular fluid-filled tank (diameter 1 m) positioned on a rotating turntable. Initially the granules were distributed in a thin, uniform layer across the entire bottom of the tank. The fluid above the layer was in a state of solid-body rotation and hence did not move relative to the granules. Pattern formation is initiated when the rotational velocity of the turntable is instantaneously increased from its original value ω_0, by a sufficiently large increment $\Delta\omega$, to a higher velocity ω_1. The fluid mass inside the tank cannot follow the instantaneous acceleration. This results in shear forces between the granule layer and the fluid above it. The granules are set in motion, slide across the bottom of the tank, and, within a few seconds, form patterns such as that shown in Fig. 1. Depending on the experimental conditions patterns displaying between $7 \leqslant n \leqslant 110$ spiral arms were observed. The spiral arms originate from a uniform, circular granule patch in the center of the tank whose radius r_0 varies with the experimental conditions. Granules located within the patch radius remain unaffected by the ongoing reorganization process on its outside.

The data we use for comparison with our results for the spiral patterns originate from experiments in four fluvial systems with substantially different flow conditions. Initially, the motivation for the comparison was to verify that the spirals do indeed represent a rotating analog of sand ripples as suggested in Ref. [9]. However, we believe that the data comparison is, in fact, of much wider interest. The extensive data sets contained in Refs. [11–16] have previously not

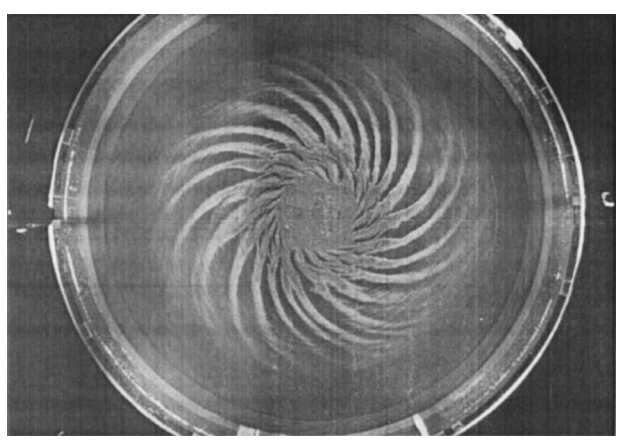

FIG. 1. Spiral-ripple pattern observed in an experiment with $\Delta\omega = 2.15\ \mathrm{rad\,s^{-1}}$, $\omega_1 = 3.16\ \mathrm{rad\,s^{-1}}$; turntable rotates clockwise. The diameter of the pattern corresponds to the diameter (1 m) of the fluid-filled circular tank.

*Electronic address: farzam@pmmh.espci.fr
†Electronic address: pjt@eng.warwick.ac.uk

 ©2003 The American Physical Society

been compared to each other. The data analysis discussed here suggests the existence of a common, universal scaling behavior governing ripple formation in all systems compared.

II. DATA COMPARISON

Our experimental data of Refs. [6–10] are compared to data for (i) steady, unidirectional flow in an annular channel [11,12] (ii) oscillating flow in an annular channel [13], (iii) steady, unidirectional flow in a straight channel [14], and (iv) oscillating flow in straight channels [15,16]. The sand-ripple patterns discussed in Refs. [11–16] are formed on relatively short time scales—typically within a few seconds. This is comparable to the formation time scale of our spiral patterns, which is approximately 10–20 s. For such short time scales the ripple wavelength emerging under oscillatory or unidirectional flow characterizes transitional and nonequilibrium states [17,18]. Thus, the discussion presented here is restricted to *transitional* ripple patterns during the early stages of their evolution.

The wavelength $\lambda_0 = 2\pi r_0/n$ appearing at the edge of the center patch of the spiral patterns is determined by the critical threshold velocity v_k required to set the granules in motion [6,9,10]. The critical velocity is given by $v_k = \text{const} \times \Delta\omega r_0$ where the constant is $O(1)$. As λ_0 develops at the critical radius r_0, corresponding to the boundary for the onset of granule motion, it must always be equal to the shortest possible wavelength the system can display [9,10]. This is an important characteristic feature of the present system. Systems (i)–(iv) do not, generally, display the shortest possible wavelength. One fundamental difference distinguishing our system from the others is the presence of background rotation in our experiments.

The comparison of the ripple wavelengths in systems (i)–(iv) of Refs. [11–16] with the spiral patterns is facilitated as follows. For the data comparison, the ripple wavelength is nondimensionalized by the granule diameter as (λ/d_G). It is displayed as a function of a mobility parameter Θ—similar to a Shields parameter—which is defined by

$$\Theta = \frac{\rho_G U^2}{g(\rho_G - \rho_F) d_G}. \tag{1}$$

In Eq. (1), ρ_G and ρ_F represent the granule and the fluid density, respectively, and g is the gravitational acceleration. U is a typical velocity scale characterizing the flow velocity above the granule layer and thus quantifies the forcing of the system. For the spiral ripples this velocity is taken as $U = \Delta\omega r_0$. In systems (ii) and (iv)—which are subject to sinusoidal forcing—it is $U = 2\pi f A$, where f is the frequency of the oscillation and A is the associated amplitude. For the remaining two systems (i) and (iii) the appropriate value is the free-stream flow velocity in the fluid above the granules.

Figures 2–5 illustrate the action of the applied nondimensionalization scheme on some typical raw data sets from Refs. [10], [14], [15], [16]. In each of the Figs. 2–5 graph (a) displays the wavelength λ as a function of the appropriate forcing velocity U, while graph (b) displays the same data in nondimensional representation.

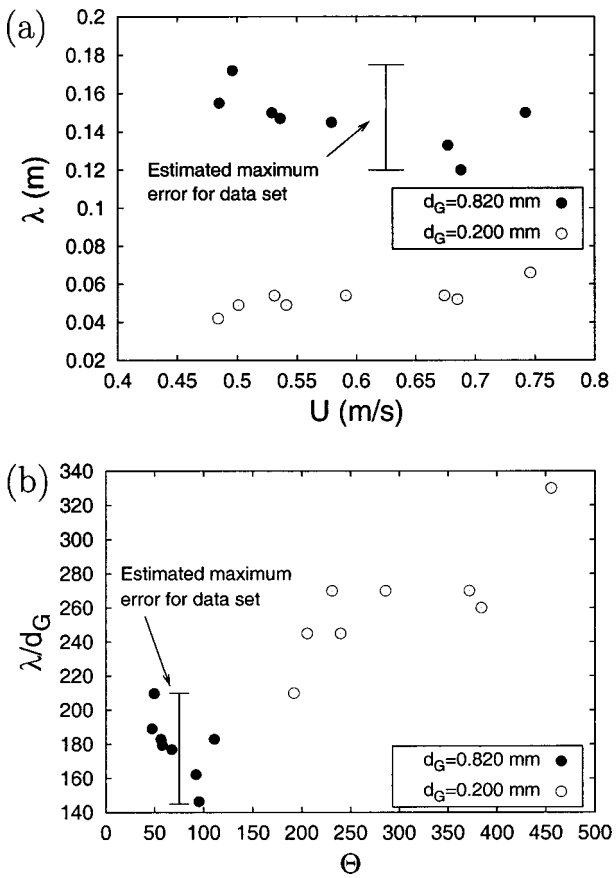

FIG. 2. Data from Ref. [14] for ripple formation under a steady flow. (a) Wavelength versus flow velocity. (b) λ/d_G versus mobility parameter Θ.

Figures 2(a)–5(a) clearly reveal that the ripple wavelength depends on the grain diameter and on the forcing velocity. Note, however, that the figures indicate that the typical measurement uncertainties associated with the data are quite substantial. The measurement errors are—generally—larger for granules with larger diameters. The estimated typical maximum errors for the larger grains are identified in each of the figures by an error bar. In Fig. 4(a), for instance, which shows data of Ref. [16], the error for the wavelength, for granules with $d_G = 1.140$ mm at flow speeds $U = 0.35\ \text{ms}^{-1}$, is $\Delta\lambda \approx \pm 0.02$ m. In nondimensional terms this corresponds to an error of $\Delta(\lambda/d_G) \approx \pm 18$. Additionally there is an uncertainty of around 15–25% for the particle diameter d_G which, for each granule sample, represents a mean value. This uncertainty for the particle size translates into errors of $\pm 14\%$ for the mobility parameter Θ. Corresponding errors are associated with all data in Refs. [6–16]. Thus, comparisons of corresponding dimensional and nondimensional representations for each of Figs. 2–5 show that, within these error margins, the nondimensionalization scheme collapses the data onto single lines.

Figure 6 displays approximately 400 data points (circles) from our experiments summarized in Ref. [10] in comparison to around 500 data points (triangles) from Refs. [11–16].

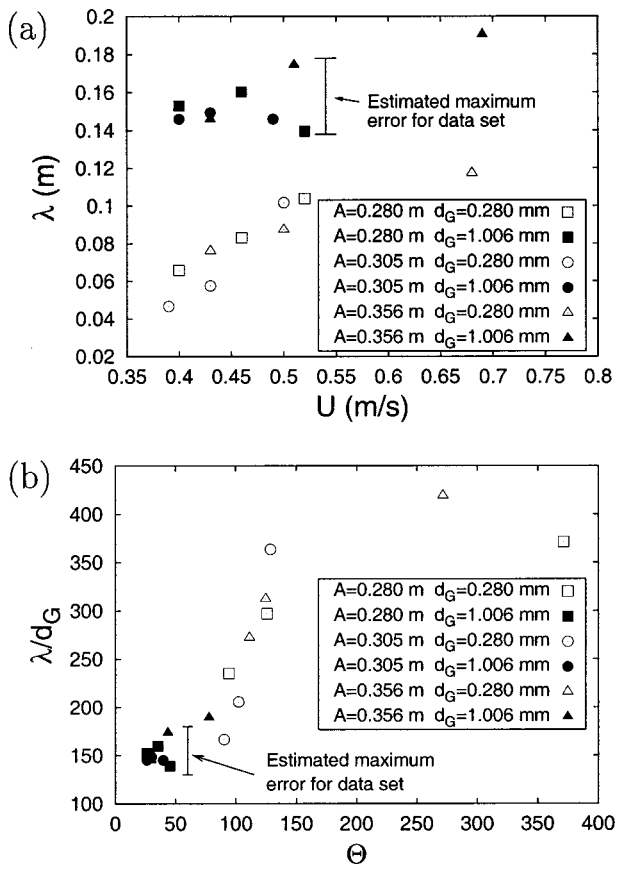

FIG. 3. Data from Ref. [15] for ripple formation under an oscillatory flow. (a) Wavelength versus flow velocity. (b) λ/d_G versus mobility parameter Θ. A represents the amplitude of the oscillations in the Manohar experiments.

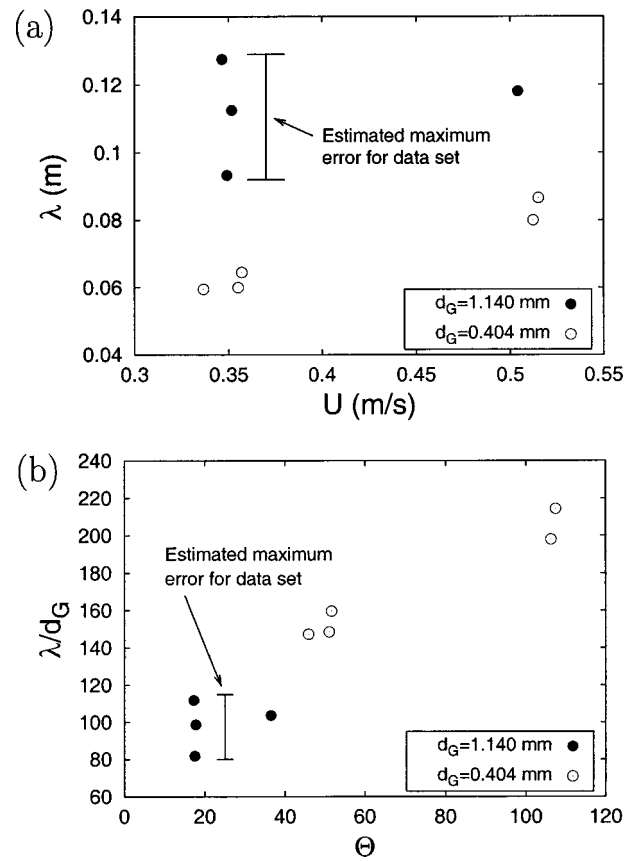

FIG. 4. Data from Ref. [16] for ripple formation under an oscillatory flow. (a) Wavelength versus flow velocity. (b) λ/d_G versus mobility parameter Θ.

The data cover parameter ranges for particle size and density of $0.110 \leqslant d_G \leqslant 3.17$ mm and $1.28 \leqslant \rho_G \leqslant 7.9$ g cm^{-3}, respectively.

Figure 6 shows that the data points of all systems collapse on one line extending over three orders of magnitude along the abscissa and two orders of magnitude along the ordinate. The data scatter in Fig. 6 can be explained in terms of the large measurement uncertainties associated with the individual raw data sets. Note that data scatter of this magnitude is typical for the type of experiments discussed here. To this end refer, for instance, to Fig. 4.4 in Ref. [3] or many other figures in Refs. [3, 4], which display data scatter of comparable magnitude to that in our Fig. 6.

The line interpolating the data in Fig. 6 represents a least-squares fit to all 900 data points. The data interpolation constitutes a linear fit of type $y = mx + b$ in the coordinates $y = \ln(\lambda/d_G)$ and $x = \ln(\Theta)$. The fitting routine yielded values of $m = 0.52 \pm 0.01$ and $b = 2.87 \pm 0.03$. This implies that $\lambda/d_G = 17.64\Theta^{0.52}$. The error estimates for m and b represent the asymptotic standard errors. These are known to be over-optimistic and should not be used for determining confidence levels, but they are useful for qualitative purposes. The errors for m and b translate into uncertainties for λ/d_G of approximately $\pm 10\%$ at $\Theta = 1000$ and $\pm 3\%$ at $\Theta = 1$.

Reference to Eq. (1) reveals that our result $\lambda/d_G \propto \Theta^{0.52}$ implies $\lambda \propto d_G^{0.48}$. This supports results of Refs. [18] and [19]. For uniform flow Ref. [18] stated that the "initial ripple length appears to be proportional to $\sqrt{d_G}$," while for oscillatory flow Ref. [19] reported that the wavelength "varies nearly as the square root of the diameter."

The data interpolation of Fig. 6 further implies that the wavelength scales with the flow velocity approximately as $\lambda \propto U$, i.e., the wavelength is proportional to the forcing of the system. It appears that this result has not been expressed in the publications on granular sand ripples referred to by us in the present paper.

The present data analysis has, in particular, shown that the data for our spiral patterns obey the same scaling one observes for sand ripples. We believe that this result constitutes an experimental verification that the spiral patterns do indeed represent a rotating analog of sand ripples in nonrotating systems. In our previous publications Refs. [6–9] we only speculated that this would be the case. The speculation was based on the observation that results obtained from a cellular automaton model together with some simple physical arguments yielded a scenario sufficient to explain experimental results revealed by one single data set consisting of approximately 50 data points. Since Refs. [6–9] did not contain any reference to or comparison with data for granular ripple formation by other authors our speculations had not been verified experimentally to date.

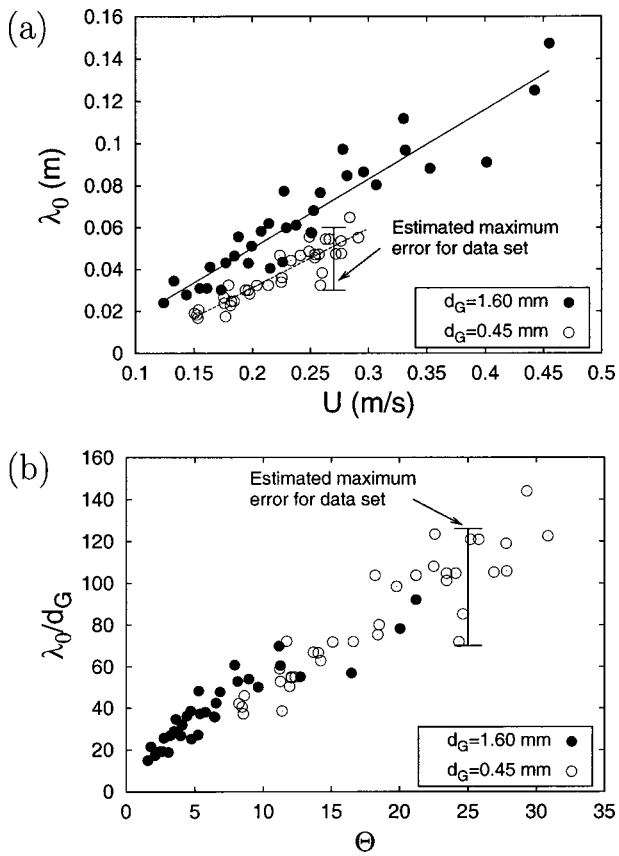

FIG. 5. Data from Ref. [10] for spiral-pattern formation. (a) The wavelength at the edge of the patch λ_0 versus the azimuthal flow velocity $r_0\Delta\omega$. (b) λ_0/d_G versus mobility parameter Θ.

Note that the experimental data for the spiral patterns of Refs. [6–10] vary more strongly with parameter variations than those for the sand ripples of Refs. [11–16]. For our spiral patterns data exist over almost the entire range of three decades $1 \leqslant \Theta \leqslant 1000$ while the data of Refs. [11–16] are confined to $\Theta > 30$. The existence of data with values substantially below $\Theta = 30$ in our rotating experiments is a consequence of the action of the centrifugal force. Our data points with lowest values of Θ represent the experiments with highest background rotation rates ω_1. For these experiments the centrifugal force alone is almost sufficient to set the granules in motion. Hence, a small additional contribution from shear forces—associated with the spin-up by the increment $\Delta\omega$—suffices to mobilize the granules and initiate pattern formation. However, a small value of $\Delta\omega$ is equivalent to small velocities U and thus corresponds to low values of Θ. In this sense one may regard the centrifugal forces as a potential means to vary and control the critical conditions for particle mobilization.

Spiral formation in our experiments of Refs. [6–10] is always initiated at the edge of the center patch. There the local conditions necessarily equal the critical conditions required to mobilize particles and initiate pattern formation. Hence, the wavelength developing at the edge of the center patch must always correspond to the smallest wavelength which the system can display. This is not so for the experiments of Refs. [11–16] where—depending on the forcing velocity—the system can display any wavelength equal to or larger than the critical onset wavelength. Consequently, for these systems the critical onset wavelength must be measured in a series of experiments by decreasing the forcing in successive small steps until, eventually, ripples no longer form. Once it becomes possible to account for and quantify the exact influences of the centrifugal force our setup of Refs. [6–10] represents a particularly convenient system to determine the critical onset wavelength for any given fluid-granule combination in one single experiment.

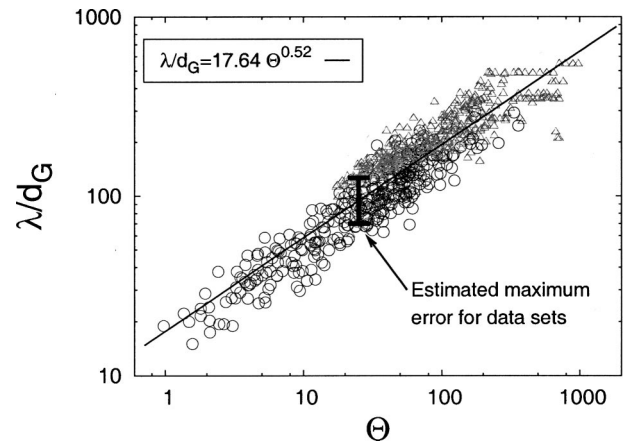

FIG. 6. Nondimensional ripple wavelength λ/d_G as a function of the Shields parameter Θ. Comparison of the spiral-pattern wavelength of Refs. [6,10] with the data of Refs. [11–16].

Furthermore, unlike other experimental configurations used to study ripple formation our system might enable a direct control of the boundary-layer thickness and hence of the shear stress. The boundary-layer flow on the bottom of our rotating tank resembles the flow over a rotating disk. The rotating disk–boundary layer is described by a similarity solution representing an exact solution of the Navier-Stokes equation. The boundary-layer thickness is constant across the region on the disk where the flow remains laminar and it scales with the background rotation rate [10,20,21]. Finally, the mobility parameter of Eq. (1) does not account for the fluid viscosity. The experiments summarized in Ref. [10] have shown that the ripple wavelength scales with the kinematic viscosity ν of the fluid as $\lambda \propto \nu^{0.25}$.

III. CONCLUSION

Experimental data for the wavelength scaling of ripple patterns emerging in five fluvial systems involving substantially different flow conditions were compared to each other.

The data comparison revealed that a common global scaling behavior governs the pattern wavelength in these systems during the early stages of ripple formation. This indicates that common physical mechanisms facilitate the onset of pattern formation in all the systems compared to each other.

The consistent wavelength scaling for the spiral patterns [6–10] and for granular ripples [11–16] verifies our speculation of Ref. [9] that the spirals represent a rotating analog of sand ripples in nonrotating systems.

[1] R. A. Bagnold, *The Physics of Blown Sand and Desert Dunes* (Methuen, London, 1941).
[2] J. R. L. Allen, *Sedimentary Structures* (Elsevier, Amsterdam, 1984).
[3] J. F. A. Sleath, *Sea Bed Mechanics* (Wiley, New York, 1984).
[4] A. J. Raudkivi, *Loose Boundary Hydraulics*, 3rd ed. (Pergamon, Oxford, 1990).
[5] N. Lancaster, *Geomorphology of Desert Dunes* (Routledge, London, 1995).
[6] P. J. Thomas, J. Fluid Mech. **274**, 23 (1994).
[7] P. J. Thomas and F. Zoueshtiagh, Album of Visualization **17**, 1 (2000).
[8] F. Zoueshtiagh and P. J. Thomas, Phys. Fluids **12**, S10 (2000).
[9] F. Zoueshtiagh and P. J. Thomas, Phys. Rev. E **61**, 5588 (2000).
[10] F. Zoueshtiagh, Ph.D thesis, University of Warwick, Coventry, U.K., 2001.
[11] A. Betat, Ph.D thesis, Otto-von-Guericke Universität, Magdeburg, Germany, 1999.
[12] A. Betat, V. Frette, and I. Rehberg, Phys. Rev. Lett. **83**, 88 (1999).
[13] M. Scherer, F. Melo and M. Marder, Phys. Fluids **11**, 58 (1999).
[14] S. E. Coleman and B. W. Melville, J. Hydraul. Eng. **122**, 301 (1996).
[15] M. Manohar, U.S. Army Beach Erosion Board Technical Memo, 1955 (unpublished).
[16] J. F. A. Sleath, J. Hydraul. Res. **14**, 69 (1976).
[17] A. Stegner and J. E. Wesfreid, Phys. Rev. E **60**, R3487 (1999).
[18] A. J. Raudkivi, J. Hydraul. Eng. **123, 1**, 58 (1997).
[19] R. A. Bagnold, Proc. R. Soc. London, Ser. A **187**, 1 (1946).
[20] H. P. Greenspan, *The Theory of Rotating Fluids* (Cambridge University Press, Cambridge, England, 1968).
[21] J. M. Owens and R. H. Rogers, *Heat Transfer in Rotating-Disc Systems Volume 1, Rotor-Stator Systems* (Research Studies Press, Taunton, 1989).